Journal of Organometallic Chemistry 1048 (2026) 124029

Contents lists available at ScienceDirect

Journal of Organometallic Chemistry

journal homepage: www.elsevier.com/locate/jorganchem

Selective recognition of ATP over phosphorylated molecules in aqueous media by urea-based arene ruthenium metalla-rectangle

Alaa Maatouk, Thibaud Rossel, Bruno Therrien *

Institute of Chemistry, University of Neuchâtel, Ave. de Bellevaux 51, Neuchâtel 2000, Switzerland

ARTICLE INFO

Keywords:
Arene ruthenium metalla-rectangle
Urea
ATP sensing
Fluorescent indicator displacement assay
Synergistic interactions
Selective recognition

ABSTRACT

Selective recognition of biomolecules is of paramount importance in medicine, biotechnology, and cellular biology. Adenosine triphosphate (ATP), the universal energy currency of living systems, represents a valuable analytical target in sensing technology. However, discriminating ATP from its closely related analogues (ADP, AMP) remains a challenge. Herein, we report the synthesis of two arene ruthenium metalla-rectangles incorporating urea-based units. These water-stable assemblies are obtained from the dinuclear complex $[Ru_2(p\text{-cymene})_2\{bis(2\text{-hydroxyethyl})oxamidate\}Cl_2]$ and the bipyridyl connectors 1,1′-(1,4-phenylene)bis{3-(pyridin-4-yl)urea} (PPU) and 1,1′-(naphthalene-1,5-diyl)bis{3-(pyridin-4-yl)urea} (NPU) in the presence of silver triflate. Both metalla-rectangles are isolated as triflate salts, with the formula $[Ru_4(p\text{-cymene})_4\{bis(2\text{-hydroxyethyl})oxamidate\}_2(PPU)_2](CF_3SO_3)_4$ (MRPPU) and $[Ru_4(p\text{-cymene})_4\{bis(2\text{-hydroxyethyl})ethanediamide\}_2(NPU)_2](CF_3SO_3)_4$ (MRNPU), respectively. Both metalla-rectangles can interact with fluorescein (FLU) to form weakly-fluorescent host-guest systems, resulting in discrete fluorescent indicator displacement assays (FIDA). The MRPPU rectangle shows in buffered aqueous solution a selective ATP recognition over purine nucleotides, as opposed to MRNPU, with an affinity of $2.4 \times 10^4\ M^{-1}$ and a detection limit of 22.0 μM. The dissimilar response of these two metalla-rectangles is rationalized from their molecular design, suggesting distinct binding interactions with ATP.

1. Introduction

Adenosine triphosphate (ATP) is an important nucleotide and the main energy carrier in living organisms [1,2]. It participates directly in vital physiological processes, including energy transfer [3], macromolecular synthesis (proteins, DNA, RNA) [4], active transport of ions in cells, cell division, muscle contraction, enzymatic activation, signal transduction, glycolysis and Krebs cycle [5–7]. Elevated or insufficient ATP levels in cells can result in the development of many diseases such as Parkinson, aggressive tumors, cancer, neurodegenerative diseases, ischemia and cardiovascular diseases [8–12]. Thus, the detection of the content and dynamic fluctuations of ATP in biological samples is of great importance in the regulation of the ATP level and the treatment of ATP-related diseases [8–12]. To date, ATP can be recognized using different techniques, including mass spectrometry (MS), high-performance liquid chromatography (HPLC), electrochemical study, bioluminescence analysis and ion chromatography [13–16]. However, these analytical methods suffer from limited sensitivity, so as an alternative, fluorescent-based probes and sensors can, not only increase sensitivity, but also offer simplicity, rapidity, low-cost fabrication, real-time detection and dynamic imaging [17,18].

Selectivity, water solubility, high affinity and appropriate detection range (1–10 mM) are the main factors to keep in mind when designing ATP sensors. ATP is composed of a ribose, an adenine base and triphosphate, each part offering sites for interactions. Coordination bonds, π–π stacking, electrostatic interactions, and hydrogen bonds, are all possible interactions between ATP and sensors. The adenine can undergo π–π stacking with planar moieties, ribose can interact with boronic acid via covalent bonding, the negatively charged phosphate provides electrostatic interactions with positively charged moieties, while complexation with metal and hydrogen bonding with urea groups can also take place. This binding diversity enhances the recognition probability and selectivity of well-designed receptor towards ATP. Based on these interactions, different types of ATP sensors have been developed, among them: chemosensors using metal ion complexes [19–22], sensors based on boronic acid [23,24], sensors based on urea derivatives

Dedicated to Professor Richard D. Adams on the occasion of his retirement.

* Corresponding author.
E-mail address: bruno.therrien@unine.ch (B. Therrien).

https://doi.org/10.1016/j.jorganchem.2026.124029
Received 5 December 2025; Received in revised form 16 January 2026; Accepted 19 January 2026
Available online 19 January 2026

[25], sensors bearing pyrenyl groups to form excimers [26,27], sensors bearing polythiophene [28], sensors containing biomolecules [29], organic small molecules [30–32], covalent organic cages [33], organic macrocycles [34,35], metalla-macrocycles [36], metal-organic frameworks [37], metalla-cages [38,39] and aptamer-Au nano-particles sensing systems [40]. According to the structural design of sensors, different mechanisms are involved in the sensing mechanism of ATP, namely: quenching/recovery of fluorescence, FRET-based displacement (Förster resonance energy transfer), ICT-based sensing (intramolecular charge transfer), PET (photoinduced electron transfer), ESIPT (excited-state intramolecular proton transfer), excimer/exciplex switching, allosteric switching, RDA (receptor displacement assay), IDA (indicator displacement assay) and host-guest interactions in supramolecular chemistry [41–44]. Nevertheless, high structural similarity exists between ATP and other nucleotides like AMP (adenosine monophosphate), ADP (adenosine diphosphate), GMP (guanosine monophosphate), GDP (guanosine diphosphate), GTP (guanosine triphosphate), etc., which prevent a selective recognition of ATP in biological media. Different sensing array strategies have been developed to target analyte discrimination in sensing, including, colorimetric sensing arrays, metal–ligand sensor arrays, polymeric microarray chips, peptide- or DNA-based arrays, nanoparticle-based colorimetric arrays [45–49]. Such platforms are usually associated to machine learning techniques, such as principal component analysis (PCA) [50,51], linear discriminant analysis (LDA) [50,52] and hierarchical cluster analysis (HCA) [53], to interpret complexed responsive patterns. Despite the power of these combinatorial methods [54–60], distinguishing ATP from other nucleotides remains challenging.

Herein, we report the synthesis and characterization of two arene-ruthenium metalla-assemblies incorporating phenyl or naphthyl urea-based linkers. These metalla-rectangles interact with fluorescein (FLU) to form two host-guest systems, which significantly reduce the natural fluorescence of FLU. Then, the recognition of phosphorylated molecules was studied in aqueous media, exploiting fluorescent indicator displacement assay (FIDA) mechanisms. The phenyl derivative (MRPPU) acts as a powerful sensor with multiple interactions for good selectivity of ATP over phosphorylated molecules, whereas the naphthyl analogue (MRNPU) is a non-specific but versatile multiple nucleotide's sensor. Our results compare favorably with those obtained from other metal-based assemblies previously used as ATP sensors.

2. Results and discussions

2.1. Synthesis and characterization of the metalla-rectangles

As illustrated in Scheme 1, metalla-rectangles MRPPU and MRNPU are synthesized in two steps from [Ru_2(*p*-cymene)$_2$\{bis(2-hydroxyethyl) oxamidate\}Cl_2] and the bipyridyl connectors 1,1′-(1,4-phenylene)bis{3-(pyridin-4-yl)urea} (PPU) and 1,1′-(naphthalene-1,5-diyl)bis{3-(pyridin-4-yl)urea} (NPU) in the presence of silver triflate (see also Schemes S1–S3). The successful formation of the metalla-rectangles is confirmed by ^{1}H, ^{13}C{^{1}H} and DOSY NMR spectroscopy, and ESI-MS spectrometry (Figures S1–S11). Despite the stereogenic nature of the Ru centers, the ^{1}H NMR spectra of MRPPU (Figure S4) and MRNPU (Figure S8) exhibit expected and well-defined signals, consistent with the anticipated coordination environment. Diffusion-ordered NMR spectroscopy (DOSY) shows the presence of discrete species, characterized by single diffusion coefficients in deuterated methanol (Figures S6 and S10). Electrospray ionization mass (ESI-MS) spectra showed multiples peaks consistent with the formation of the metalla-rectangles MRPPU (m/z = 497.1 [MRPPU - 4$CF_3SO_3^-$]$^{4+}$, 712.1 [MRPPU - 3$CF_3SO_3^-$]$^{3+}$, 1142.8 [MRPPU - 2$CF_3SO_3^-$]$^{2+}$; Figure S7) and MRNPU (m/z = 522.2 [MRNPU - 4$CF_3SO_3^-$]$^{4+}$, 745.8 [MRNPU - 3$CF_3SO_3^-$]$^{3+}$, 1193.1 [MRNPU - 2$CF_3SO_3^-$]$^{2+}$; Figure S11).

In terms of solubility, MRPPU and MRNPU exhibit high solubility in hydrogen-bond donating or accepting solvents, including methanol, ethanol, acetone. In water, MRPPU and MRNPU show solubility at low μM concentrations, which make them suitable for sensing biomolecules in aqueous media. The water solubility is associated to the different building blocks used to prepare the metalla-rectangles and the tetracationic nature of the metalla-assemblies. Despite being prone to form hydrogen-bonds with solvent, the diaryl urea units parallel to each other can instead favor intramolecular hydrogen-bonds, where two adjacent N–H groups from one linker interact with the carbonyl groups of the parallel linker. This self-association phenomenon can potentially reduce the availability of binding sites to analytes [61]. However, by inserting

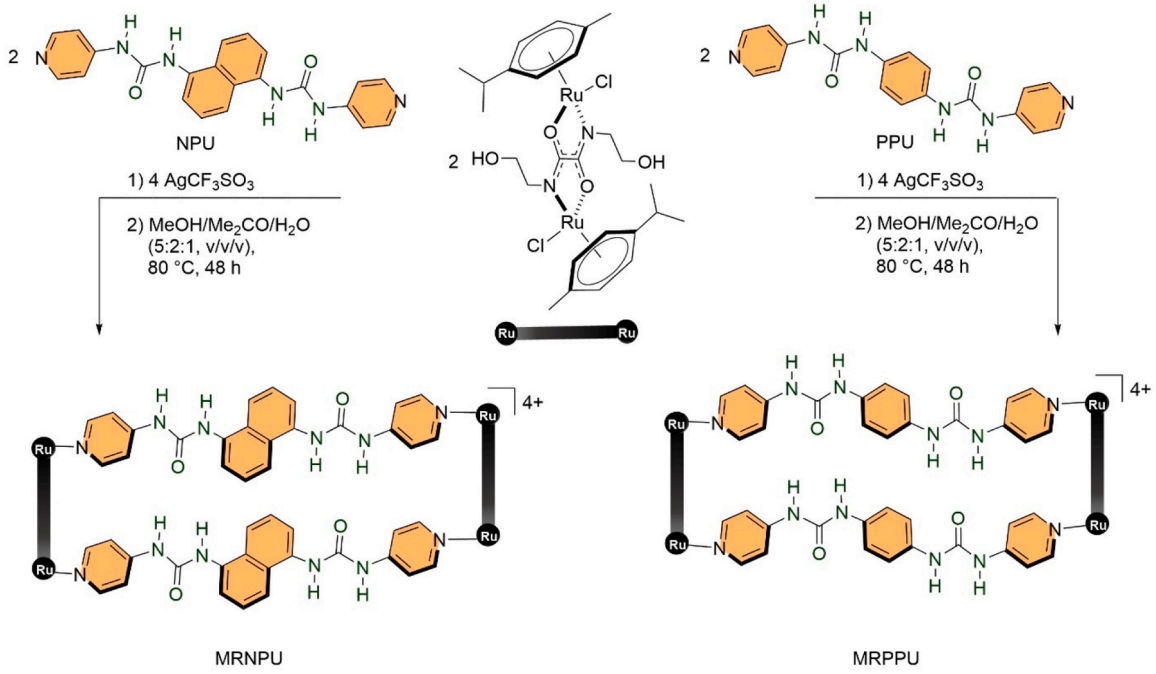

Scheme 1. Schematic illustration for the synthesis of metalla-rectangles MRPPU and MRNPU.

the diaryl urea units in a discrete supramolecular structure the self-association is somehow limited [62], thus keeping intermolecular binding capacity for guest molecules.

2.2. Fluorescein binding with metalla-rectangles

Fluorescein (FLU) is a commercial dye largely used in supramolecular chemistry for host–guest monitoring purposes due to strong emission, good solubility in aqueous media, and well-defined photophysical properties [63–65]. Fluorescein has a compact and planar structure with hydrophilic and hydrophobic characters, being a suitable guest for metalla-assemblies [66]. At physiological pH, FLU is mainly under its dianionic form FLU^{2-}, increasing its hydrophilic character [67]. The level of fluorescence quenching is impacted by the complementarity size of the host-guest system and the nature of the interactions involved. MRPPU and MRNPU provide multiple binding sites from the urea groups on the linkers to the hydroxyl groups on the clips, all having the possibility to interact with FLU^{2-}, as well as the aromatic rings through π-π stacking interactions (Fig. 1a). In addition, the ideal size complementarity between metalla-rectangles and FLU^{2-} can also allow in-core encapsulation [75]. Therefore, inside the cavity or peripheral interactions can both result in FLU^{2-} – metalla-rectangle host-guest systems (Fig. 1b), which can overall modify the fluorescence intensity of fluorescein.

Multiple titrations experiments were performed to estimate the binding constant and stoichiometry between the metalla-rectangles and FLU^{2-} (Fig. 2, and SI). Gradual addition of MRPPU and MRNPU (0–75 μM) to a solution of FLU (12.5 μM) in HEPES buffer pH 8 resulted in a rapid decrease in the fluorescence intensity (Fig. 2a and 2b). Total quenching of the fluorescence was achieved with 1.5 equiv. of MRPPU (99.9 %), whereas 2.5 equiv. of MRNPU were needed to produce a similar effect (98.4 %). These initial fluorescence titrations provide binding constants of $7.6 \pm 2.0 \times 10^5\ M^{-1}$ between FLU^{2-} and MRPPU (Fig. 2a) and $1.6 \pm 0.6 \times 10^5\ M^{-1}$ for FLU^{2-} and MRNPU (Fig. 2b). The titrations were performed under conditions where MRRPU and MRNPU are in excess, thus favoring 1:1 systems [66]. Therefore, reversed titrations involving an excess of FLU were also performed. The titration of MRPPU (12.5 μM) and MRNPU (12.5 μM) with an increasing concentration of FLU (0–25 μM) in HEPES buffer pH 8 shows a bilinear fitting with an inflexion point at respectively 12.5 μM for MRPPU (Fig. 2c) and 15 μM for MRNPU (Fig. 2d). These results confirm that FLU^{2-} binds to MRPPU in a 1:1 stoichiometry, while for MRNPU, a different stoichiometry takes place, thus requiring a more in-depth analysis.

Job plots were conducted in HEPES buffer pH 8, by combining different mole fractions of FLU and metalla-rectangles, thus revealing that FLU^{2-} binds to MRPPU in a 1:1 ratio (Fig. 2e) and MRNPU in a 2:1 ratio (Fig. 2f). To further strengthen the estimated stoichiometry and better understand the FLU^{2-}·MR interactions, various ^1H and DOSY NMR experiments were carried out at 25 °C in MeOD (Figures S12–S13). In the presence of FLU, significant variations of the chemical shift, peak's shape and multiplicity were observed for several signals (Figures S12a and S13a). Interestingly, the ^1H NMR signals of FLU around 6.5 ppm and 7.7 ppm are attenuated with MRPPU, while they remain fully visible with MRNPU, suggesting different binding dynamics. Indeed, a DOSY NMR experiment of FLU and MRPPU exhibits a single diffusion coefficient (Figure S12b), indicating a FLU⊂MRPPU host-guest system. In contrast, the DOSY of FLU and MRNPU reveals two distinct diffusion coefficients (Figure S13b), indicating that FLU interacts weakly with

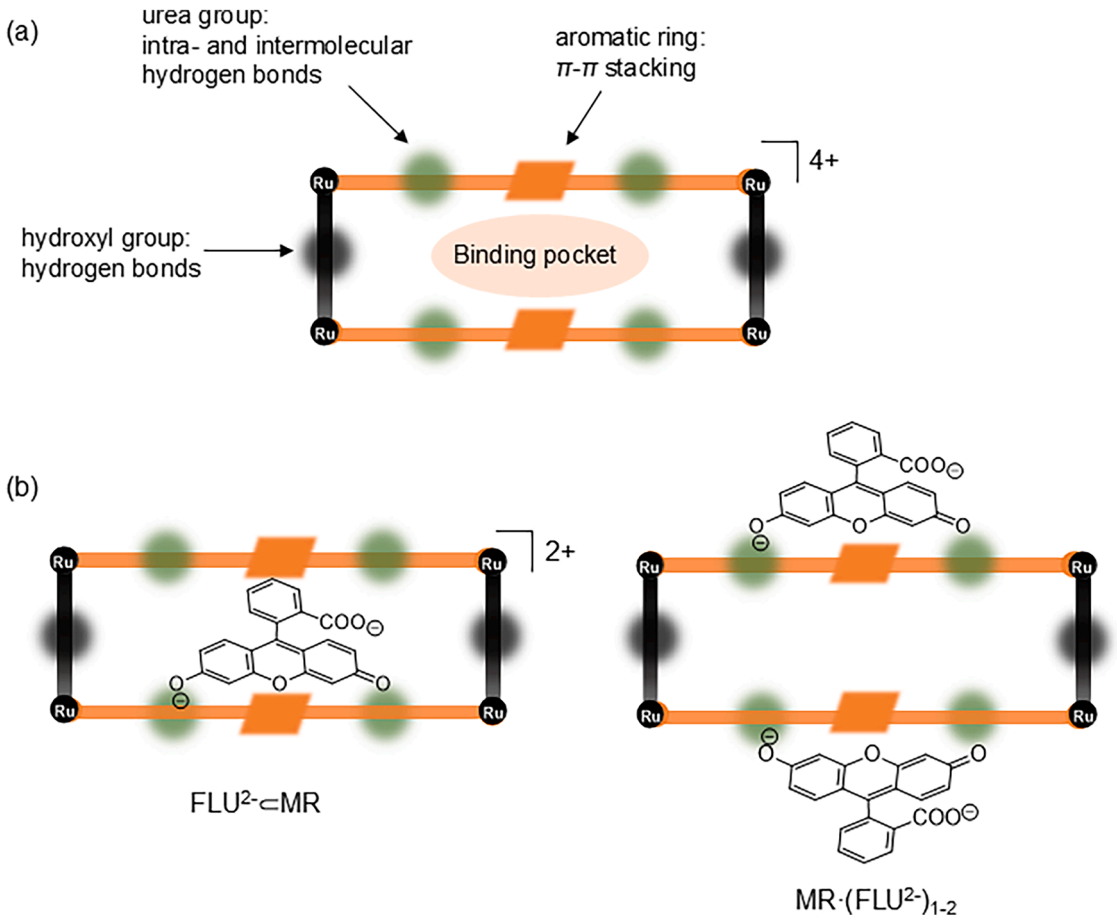

Fig. 1. (a) Schematic representation of possible interactions between the metalla-rectangles (MR) and the dianionic form of fluorescein (FLU^{2-}); (b) inside and outside the cavity of MR.

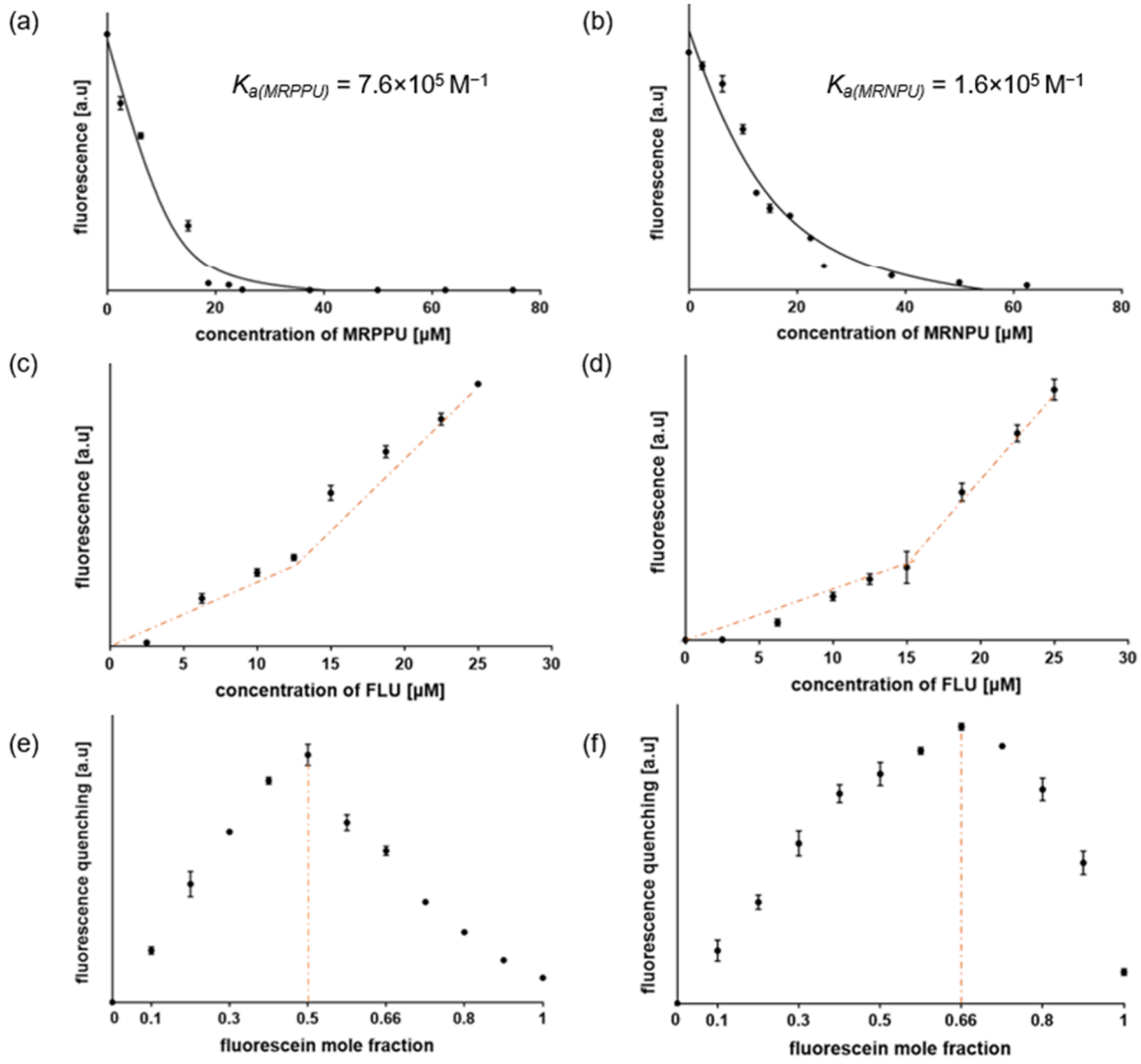

Fig. 2. Spectroscopic titrations (λ_{ex} = 498 nm, λ_{em} = 515 nm) in HEPES buffer pH 8 of: (a) FLU (12.5 μM) with MRPPU (0–75 μM); (b) FLU (12.5 μM) with MRNPU (0–75 μM); (c) MRPPU (12.5 μM) with FLU (0–25 μM); (d) MRNPU (12.5 μM) with FLU (0–25 μM). Job plots in HEPES buffer pH 8 based on fluorescence quenching (λ_{ex} = 498 nm, λ_{em} = 515 nm) of a mixture containing different molar ratios of MR and FLU keeping total concentration constant at 12.5 μM of: (e) FLU + MRPPU; (f) FLU + MRNPU.

MRNPU in deuterated methanol.

2.3. Sensing of phosphorylated molecules

Having demonstrated the ability of FLU^{2-} to interact with MRPPU and MRNPU with significant fluorescence quenching, the two host-guest systems were used as fluorescent indicator displacement assays for the detection of phosphorylated molecules [68]. Since the skeleton of MRPPU and MRNPU contains urea groups, it can be assumed that phosphorylated biomolecules will be able to interact with the metalla-rectangles and potentially displace FLU^{2-} in both systems (Scheme 2). Three types of phosphorylated molecules were selected, phosphorylated nucleosides, phosphorylated sugars and phosphorylated anions (Fig. 3).

Analyte screening was performed to evaluate the sensing ability and selectivity of $FLU^{2-}\subset$MRPPU and FLU^{2-}•MRNPU towards phosphorylated molecules. All experiments were conducted at 25°C in HEPES buffer pH 8, by mixing FLU and MRPPU or MRNPU in a 1:1 ratio (12.5 μM), leading to a decrease in the fluorescence signal (45 % with MRPPU and 55 % with MRNPU). Subsequently, each individual analyte was added in excess (40 equiv.), and the fluorescence measured 10 minutes later (Fig. 4). Both sensing systems $FLU^{2-}\subset$MRPPU and FLU^{2-}•MRNPU show no fluorescence recovery upon addition of phosphorylated sugars, as well as with adenine (a) and guanine (b) (Fig. 4). However, for other phosphorylated molecules the responses differ with the sensor.

Indeed, with pyrimidines (c-e), phosphorylated purines (1a-3b), phosphorylated pyrimidines (3c-e) and phosphorylated anions (7–9), the FLU^{2-}•MRNPU system shows almost full recovery of the fluorescence (Fig. 4), while with $FLU^{2-}\subset$MRPPU only pyrimidines (c-e), adenosine trisphosphate (3a), pyrimidine-triphosphates (3c-e) and triphosphate (9) show partial fluorescence recovery. In particular, the fluorescence recovery is stronger for uracil (d) and thymine (e) than for cytosine (c), and among purines, only adenosine triphosphate (ATP) has positive fluorescence recovery (44%). These results show a degree of selectivity in $FLU^{2-}\subset$MRPPU for triphosphate derivatives, while FLU^{2-}•MRNPU is a non-specific phosphorylated molecules sensor.

According to the literature, it is difficult to discriminate between nucleotides due to the great similarity between structures [69,70]. Some systems show selective recognition of nucleotides by controlling the structure of the sensor to detect either a determined number of phosphate units (mono-, di-, tri-) [71,72], the type of nucleobase [73], or both, specific number of phosphates and specific nucleobase

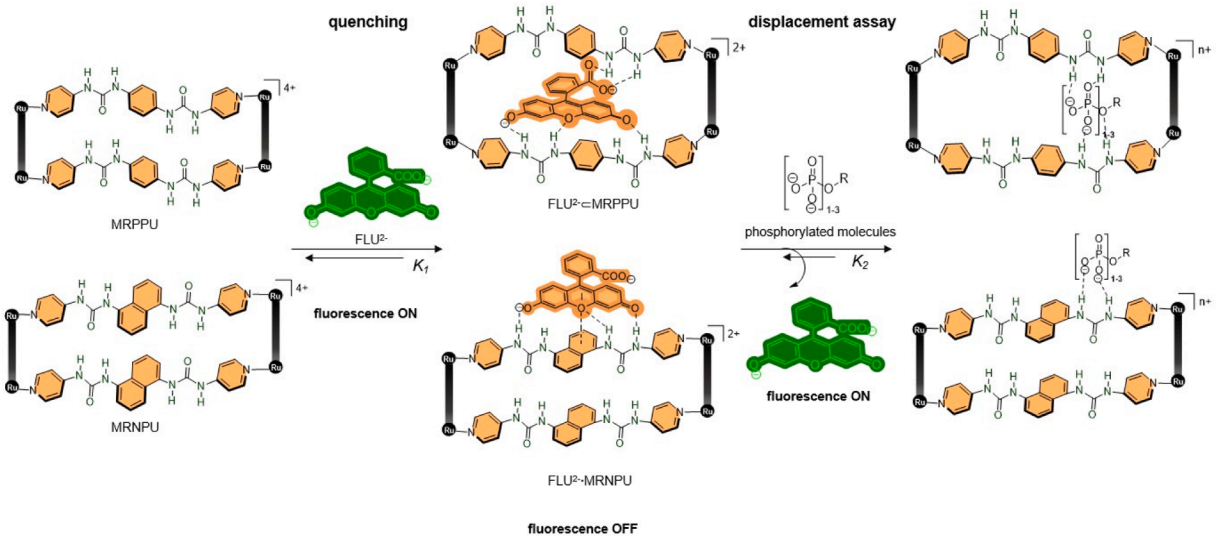

Scheme 2. Schematic representation of the fluorescent indicator displacement assay (FIDA) for phosphorylated molecules involving MRPPU (top) and MRNPU (bottom).

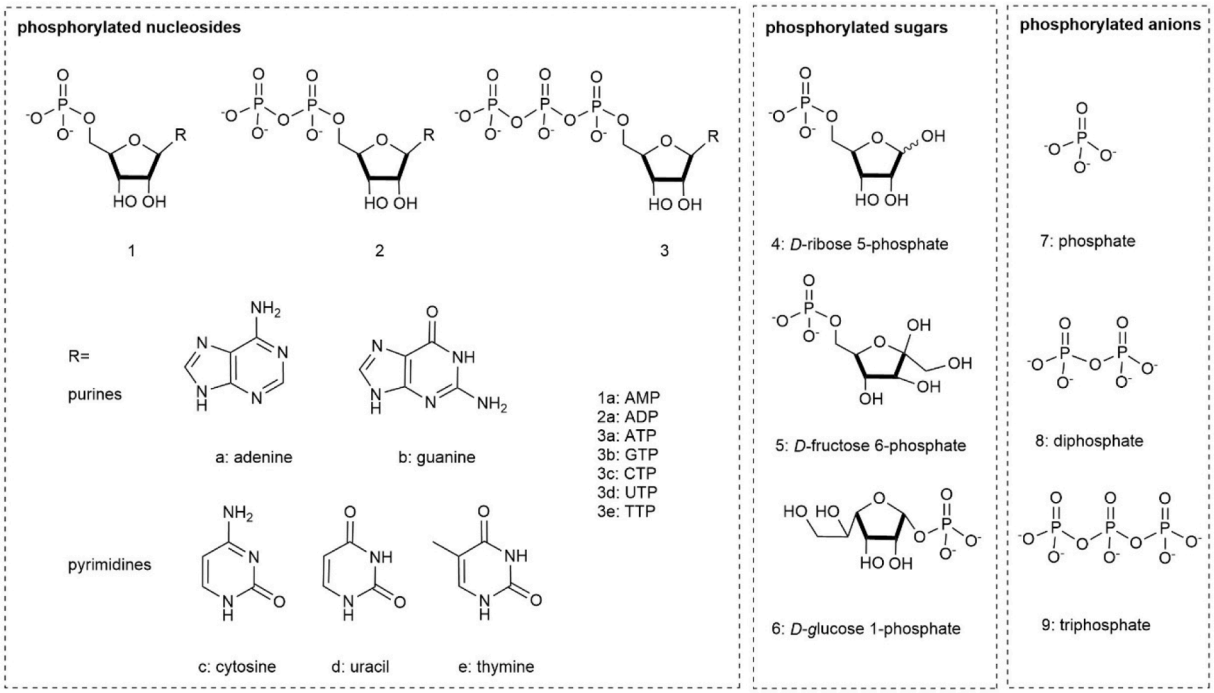

Fig. 3. Chemical structures of phosphorylated nucleosides (categorized by their a–e bases), phosphorylated sugars and phosphorylated anions.

components [69,70,74]. In the case of FLU^{2-}⊂MRPPU, the detection of phosphorylated molecules seems to mainly rely on triphosphate, with however an interesting variation in the intensity of the fluorescence recovery linked to the nucleoside involved. Therefore, this particular behavior associated with triphosphate and nucleoside, can be exploited for selective recognition.

2.4. Binding constants and mechanisms

To better understand the binding interaction, affinity and selectivity between the two systems and analytes, titration experiments were performed in HEPES buffer pH 8, by monitoring the fluorescence upon increasing concentration of analytes (see experimental section). The titration profiles obtained with FLU^{2-}⊂MRPPU and FLU^{2-}•MRNPU show different characteristics: For FLU^{2-}•MRNPU (Figs. 5 and S14), all analytes show hyperbolic titration curves, thus suggesting a typical displacement assay, while for FLU^{2-}⊂MRPPU, mixed responses are observed (Fig. 6), consistent with either an allosteric and/or a displacement assay. In FLU^{2-}•MRNPU (Figure S14), all responses are similar. The analyte rapidly displaces FLU^{2-} from MRNPU, with a sharp increase in fluorescence at the beginning of the titration, reflecting the high affinity of MRNPU to phosphorylated molecules. Only three to four equiv. of analyte are needed to reach the equilibrium and regain full fluorescence. These titrations exhibit binding affinity in the range of 10^5 M^{-1}, following the order: (ATP, GTP) > (AMP, ADP, GMP, GDP) > (mono-, di-, tri-phosphate) (Table 1). These results confirm that $K_2 >> K_1$ ($K_{a(MRNPU)}$ = 1.6 × 10^5 M^{-1}) (Scheme 2, Fig. 2) for all analytes, meaning that the equilibrium is strongly shifted towards the formation

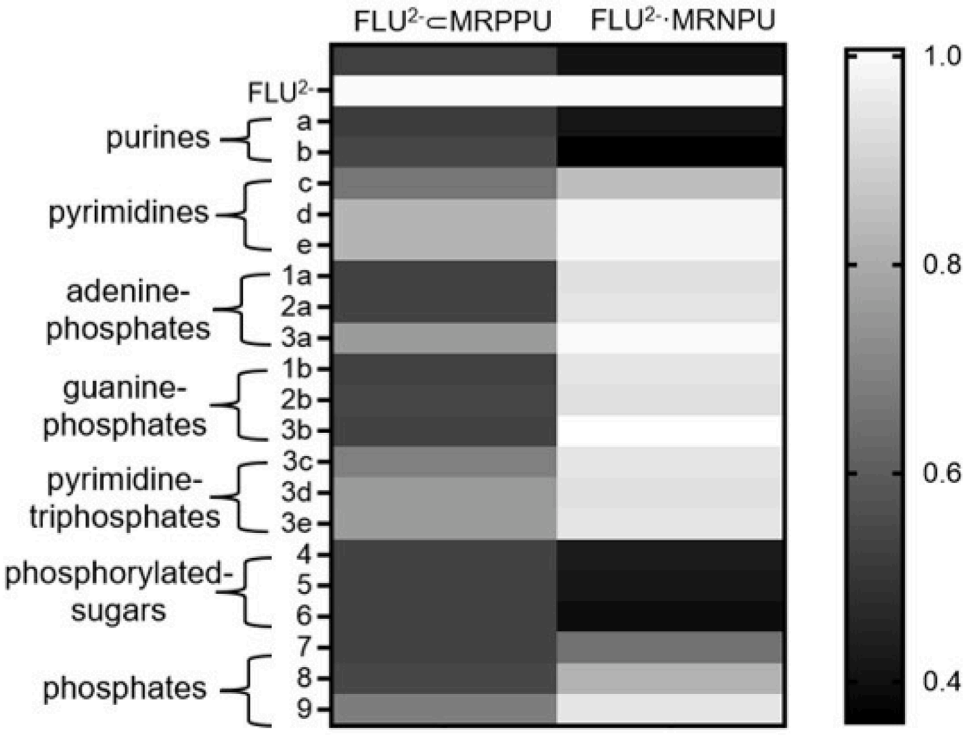

Fig. 4. Heat map of the average fluorescence intensities, FLU alone being fixed at 1 (white), upon addition of 40 equiv. of analytes in HEPES buffer pH 8: (left) $FLU^{2-}\subset$MRPPU (12.5 μM); (right) FLU^{2-}•MRNPU (12.5 μM). Darker areas indicate lower intensities (fluorescence quenching) and lighter areas higher fluorescence intensities (fluorescence recovery).

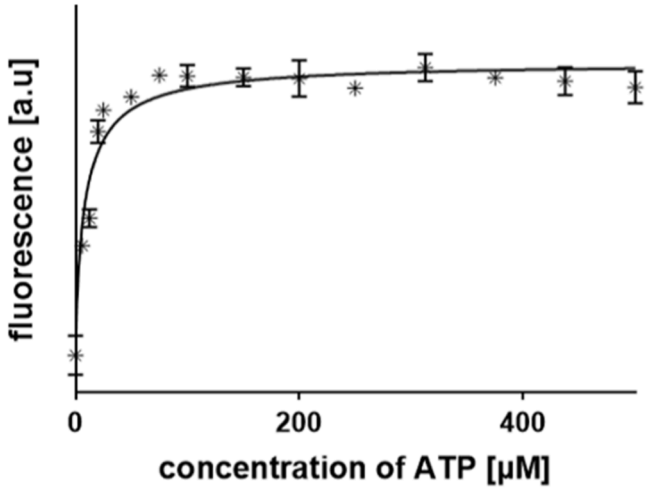

Fig. 5. Spectroscopic titrations (λ_{ex} = 498 nm, λ_{em} = 515 nm) of ATP in the presence of FLU^{2-}•MRNPU (12.5 μM) in HEPES buffer pH 8.

of analyte•MRNPU complexes.

In contrast, $FLU^{2-}\subset$MRPPU presents distinct responses with analytes (Fig. 6). ATP showed a clear displacement assay (Fig. 6a), whereas triphosphate demonstrated an allosteric recognition process resulting in a sigmoidal titration curve (Fig. 6b). The displacement of FLU^{2-} by ATP reaches the equilibrium after addition of 25 equiv., which is late by comparison with FLU^{2-}•MRNPU, suggesting that FLU^{2-} is not easily displaced from MRPPU due to its encapsulation inside the metalla-rectangle. The affinity of MRPPU for ATP was calculated following a 1:1 binding model and was determined to be $2.4 \pm 0.5 \times 10^4$ M^{-1}. The value is not significantly higher than that of MRPPU ($K_{a(MRPPU)} = 7.6 \pm 2.0 \times 10^5$ M^{-1}, Fig. 2), suggesting an incomplete displacement of FLU^{2-} by ATP, which can explain the partial recovery of fluorescence. Regarding the allosteric recognition of triphosphate, no full recovery of fluorescence was observed, even after reaching a plateau. This is normal for an allosteric mechanism [75], where the triphosphate is not kicking out FLU^{2-} from the cavity, despite strong interactions with MRPPU, only disrupting the fluorescence intensity of the $FLU^{2-}\subset$MRPPU system. The affinity of MRPPU for triphosphate was calculated following a cooperative binding model and was determined to be $2.3 \pm 0.1 \times 10^3$ M^{-1}, which is significantly lower than $K_{a(MRPPU)}$ ($K_1 > K_2$; Scheme 2).

A further evaluation of the two systems was performed using the linear range response and the limit of detection (LOD). Regarding the $FLU^{2-}\subset$MRPPU system, a good linear correlation ($R^2 > 0.99$) was observed over the concentration range of 100 − 300 μM for ATP, 370–500 μM for triphosphate, 100–250 μM for thymine, 50–200 μM for UTP and 50–250 μM for TTP (Table S1, Figure S16a). The limit of detection was estimated to be 22.0 μM for ATP and 251.4 μM for triphosphate and <100 μM for the other analytes (CTP, UTP, TTP, cytosine, uracil, thymine) (Table S1, Figure S17a). These results confirm a moderate discriminative ability of the $FLU^{2-}\subset$MRPPU sensing system and high sensitivity in the low micromolar range for ATP. Similarly, FLU^{2-}•MRNPU sensing system show a good linear correlation for the vast majority of analytes ($R^2 > 0.99$), while the linear range was not determined for AMP, ATP, diphosphate, triphosphate, CTP and TTP due to the poor correlation $R^2 < 0.98$ (Table S2, Figure S16b). A comparable limit of detection for all tested analytes was observed, indicating that the FLU^{2-}•MRNPU system lacks the ability to discriminate between analytes even at low concentration (Table S2, Figure S17b).

2.5. Comparison of metalla-cage sensors for ATP

The use of metal-based assemblies as ATP sensors remains underdeveloped. However, some reports in the literature have shown promising results. Compared to the metalla-helical triangles (**MC1, MC2**) built from cobalt(II) [38] and the platinum-based hexagonal

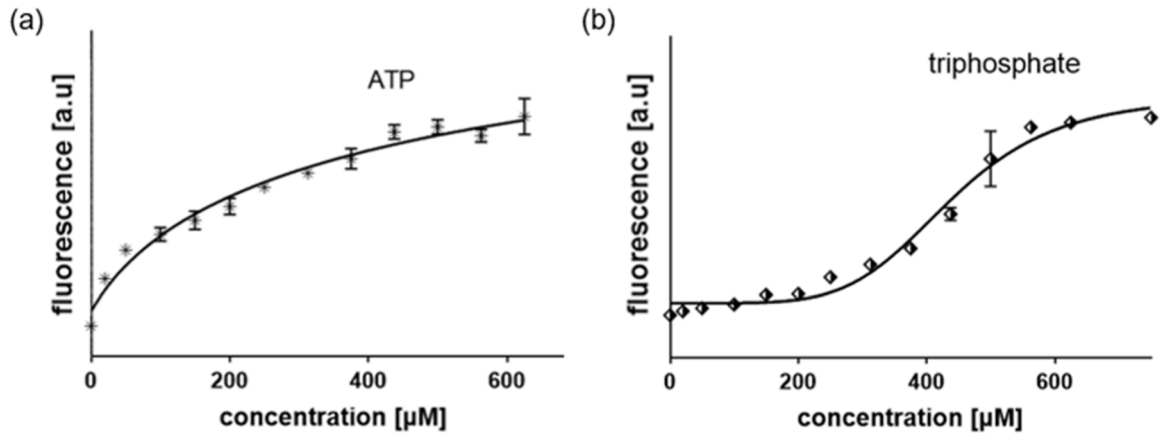

Fig. 6. Spectroscopic titrations (λ_{ex} = 498 nm, λ_{em} = 515 nm) of ATP (a) and triphosphate (b) in the presence of $FLU^{2-}\subset$MRPPU (12.5 μM) in HEPES buffer pH 8.

Table 1
Association constants (K_a) of $FLU^{2-}\subset$MRPPU and FLU^{2-}·MRNPU for the phosphorylated molecules. K_a values were determined from the data of fluorescence titrations and estimated using nonlinear regression fitting with GraphPad Prism [76]. Measurements were performed using 12.5 μM solutions of $FLU^{2-}\subset$MRPPU or FLU^{2-}·MRNPU in HEPES buffer pH 8.

phosphorylated molecule	K_a [M^{-1}] with $FLU^{2-}\subset$MRPPU	K_a [M^{-1}] with FLU^{2-}·MRNPU
cytosine [c]	$5.3 \pm 1.6 \times 10^4$	$2.6 \pm 0.4 \times 10^5$
uracil [d]	$2.4 \pm 0.8 \times 10^4$	$3.9 \pm 0.6 \times 10^5$
thymine [e]	$5.4 \pm 1.1 \times 10^4$	$2.6 \pm 0.3 \times 10^5$
AMP [1a]	n.d	$6.3 \pm 0.9 \times 10^5$
ADP [2a]	n.d	$6.0 \pm 0.9 \times 10^5$
ATP [3a]	$2.4 \pm 0.5 \times 10^4$	$1.3 \pm 0.2 \times 10^6$
GMP [1b]	n.d	$5.7 \pm 0.7 \times 10^5$
GDP [2b]	n.d	$5.3 \pm 0.5 \times 10^5$
GTP [3b]	n.d	$9.4 \pm 1.3 \times 10^5$
CTP [3c]	$5.5 \pm 1.6 \times 10^4$	$5.5 \pm 0.8 \times 10^5$
UTP [3d]	$1.8 \pm 0.5 \times 10^4$	$5.7 \pm 1.0 \times 10^5$
TTP [3e]	$7.4 \pm 2.2 \times 10^3$	$3.9 \pm 0.5 \times 10^5$
phosphate 7	n.d	$1.2 \pm 0.3 \times 10^5$
diphosphate 8	n.d	$2.8 \pm 0.5 \times 10^5$
triphosphate 9	$2.3 \pm 0.1 \times 10^3$	$4.1 \pm 0.6 \times 10^5$

metalla-prism (**4c**) [39] (Fig. 7), our metalla-sensor $FLU^{2-}\subset$MRPPU demonstrates several key advantages (Table 2). It exhibits a high affinity for ATP in water, with a binding constant in the range of 10^4 M^{-1}, with a detection limit of 22.0 μM and a wide linear range (100 – 300 μM). On the other hand, the metalla-based systems **MC1, MC2** and **4c** require organic co-solvents or operate in non-aqueous conditions. In addition, the synthesis of our sensing system is straightforward, and the $FLU^{2-}\subset$MRPPU adduct is stable in aqueous media, thus being ideal for biological applications.

3. Conclusion

We have successfully synthesized and characterized two water-soluble urea-based arene ruthenium metalla-rectangles for the recognition of phosphorylated molecules. The MRPPU and MRNPU metalla-rectangles have shown a great ability to interact with fluorescein (FLU), showing however different mode of interactions between the dye and the metalla-rectangles. Interestingly, at pH 8, FLU^{2-}·MRNPU only acts as a fluorescent indicator displacement assay (FIDA) with specific analytes, while $FLU^{2-}\subset$MRPPU shows both, allosteric and FIDA responses. This different behavior allows the $FLU^{2-}\subset$MRPPU system to show a degree of selectivity for ATP, thus highlighting the versatility of arene ruthenium metalla-assemblies in sensing.

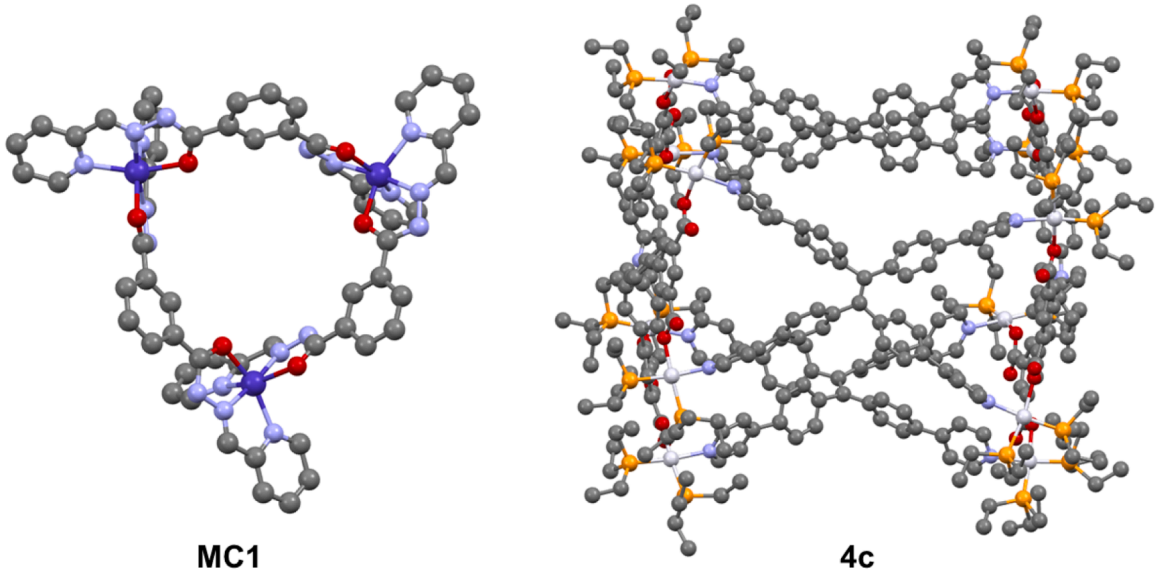

Fig. 7. Molecular structures of the cobalt-based metalla-helical triangle **MC1** [38] and the platinum-based metalla-prism **4c** [39].

Table 2
ATP sensing from metalla-cage systems reported in the literature and from this work, including the type of interactions, method used, mechanism of sensing, solvent used, selectivity, K_a [M^{-1}], linear range [μM], and LOD [μM] for ATP.

sensing system	metalla-cage/ metal center/ active group in sensing	interaction	method used	mechanism	solvent	selectivity	K_a [M^{-1}]	linear range [μM]	LOD [μM]
MC1 [39]	metalla-helical triangle/Co(II)	electrostatic	UV-vis	Werner-type encapsulation (host-guest system)	8:2 DMF/ H_2O	ATP (over nucleotides)	355	n.d	n.d
MC2 [39]	metalla-helical triangle/Co(II) sulfonamide	H-bonds	UV-vis	Werner-type encapsulation (host-guest system)	8:2 DMF/ H_2O	ATP (over nucleotides)	7200	n.d	n.d
4c [38]	hexagonal metalla-prism/Pt (II)	electrostatic	fluorescence	photoinduced electron transfer (PET)	1:1 ACN/ H_2O	ATP, ADP (over ATP, ADP, AMP)	n.d	0–100	1.16
FLU^{2-}⊂ MRPPU	metalla-rectangle/ Ru(II) urea	H-bonds	fluorescence	fluorescence indicator displacement assay (FIDA)	H_2O/ HEPES buffer pH 8	ATP (over purines)	24000	100–300	22.0

4. Experimental part

4.1. Materials and reagents

All reagents and chemicals were obtained from Sigma Aldrich or Chemie Brunschwig AG® (Basel, Switzerland) and used without further purification. All analytes were purchased from Sigma Aldrich, including: fluorescein (free acid), adenine, guanine, cytosine, uracil, thymine, trisodium phosphate, tetrasodium diphosphate, pentabasic sodium triphosphate, *D*-ribose 5-phosphate disodium, *D*-fructose 6-phosphate disodium, *D*-glucose 1-phosphate disodium, adenosine 5′-monophosphate disodium, adenosine 5′-diphosphate trisodium, adenosine 5′-triphosphate tetrasodium, guanosine 5′-monophosphate disodium, guanosine 5′-diphosphate trisodium, guanosine 5′-triphosphate tetrasodium, cytidine 5′-triphosphate tetrasodium, uridine 5′-triphosphate tetrasodium, thymidine 5′-triphosphate tetrasodium. The dinuclear arene ruthenium metalla-clip [Ru_2(*p*-cymene)$_2${*N,N′*-bis(2-hydroxyethyl)oxamidate}Cl_2] [77] and the ligand 1,1′-(1,4-phenylene)bis(3-(pyridin-4-yl) urea) (PPU) [62] were synthesized following previously reported procedures.

4.2. Instrumentation

The ^{1}H, ^{13}C{^{1}H} and DOSY NMR spectra were recorded on a Bruker Avance II 600 MHz at 23°C in MeOD and DMSO-d_6 and referenced relative to residual solvents, at 3.3 and 2.5 ppm respectively. Multiplicities are reported in Hz as: s = singlet, d = doublet, t = triplet, q = quartet and m = multiplet. Electrospray ionization mass spectra were obtained in positive ion mode on an LTQ Orbitrap Elite instrument at the ISIC Mass Spectrometry Service (SSMI) in Lausanne (Switzerland). Fluorescence measurements were carried out in black NUNC® 96 well plates using a VICTOR® Nivo™ multimode plate reader.

4.3. Synthesis and characterization

Synthesis of 1,1′-(naphthalene-1,5-diyl)bis(3-(pyridin-4-yl)urea) (NPU) (Scheme S1)

A solution of 1,5-diisocyanatonaphthalene (0.3 g, 1.4 mmol) in anhydrous THF (12 mL) was added dropwise to a solution of 4-aminopyridine (0.3 g, 3.1 mmol) in anhydrous THF (7 mL) under a nitrogen atmosphere. The mixture was stirred overnight at rt. The precipitate was collected by filtration, washed with THF and H_2O to afford pure NPU with a yield of 71.4% (0.4 g, 1 mmol). Chemical formula: $C_{22}H_{18}N_6O_2$. MW = 398.2 g·mol^{-1}.

^{1}H NMR (600 MHz, DMSO-d_6) δ 9.5 (s, 2H, NH), 8.9 (s, 2H, NH), 8.4 (m, 4H, $CH_{pyridyl}$), 8.0 (dd, J = 7.5, 0.9 Hz, 2H, $CH_{naphtyl}$), 7.9 (d, J = 8.6 Hz, 2H, $CH_{naphtyl}$), 7.6 (dd, J = 8.5, 7.5 Hz, 2H, $CH_{naphtyl}$), 7.5 (m, 4H, $CH_{pyridyl}$). ^{13}C{^{1}H} NMR (151 MHz, DMSO-d_6) δ 152.6 ($C_{pyridyl}$), 150.2 (NH-**(C**=O**)**-NH), 146.5 ($C_{naphtyl}$), 134.2 ($C_{naphtyl}$), 127.1 ($C_{naphtyl}$), 125.7 ($C_{naphtyl}$), 118.5 ($C_{naphtyl}$), 117.2 ($C_{pyridyl}$), 112.3 ($C_{naphtyl}$). ESI−MS: m/z = 399.1 [M - H]$^+$.

Synthesis and characterization of the metalla-assembly MRPPU (Scheme S2):

A mixture of [Ru_2(*p*-cymene)$_2${*N,N′*-bis(2-hydroxyethyl)oxamidate}Cl_2] (50 mg, 69.8 μmol) and $AgCF_3SO_3$ (35.7 mg, 139.7 μmol) in anhydrous MeOH (5 mL) was stirred at rt for 2 h. The resulting suspension was then filtered to remove the precipitated AgCl. Subsequently, a solution of 1,1′-(1,4-phenylene)bis(3-(pyridin-4-yl)urea) (PPU) (24.3 mg, 69.8 μmol) in a 55 mL solvent mixture of MeOH/ Me_2CO/H_2O (5:2:1, v/v/v) was added to the filtrate. The reaction mixture was heated to 80°C and stirred for 48 h. After completion, the solvent was removed under reduced pressure, and the crude product was dissolved in MeOH (2 mL). Slow addition of Et_2O induced precipitation of the target complex as a bright brown-green solid, 98% yield (88 mg, 34.1 μmol). Chemical formula: $C_{92}H_{108}F_{12}N_{16}O_{24}Ru_4S_4$. MW = 2584.3 g·mol^{-1}.

^{1}H NMR (600 MHz, MeOD) δ 7.8 (t, 8H, $CH_{pyridyl}$), 7.3 (d, J = 5.7 Hz, 8H, CH_{phenyl}), 7.0 (d, J = 2.8 Hz, 8H, $CH_{pyridyl}$), 6.0 (d, J = 6.0 Hz, 4H, $CH_{p\text{-}cym}$), 5.8 (d, J = 6.0 Hz, 4H, $CH_{p\text{-}cym}$), 5.4–5.3 (m, 8H, $CH_{p\text{-}cym}$), 4.1–3.8 (m, 16H, CH_2), 2.8–2.7 (m, 4H, C**H**$(CH_3)_2$), 1.7 (s, 12H, CH_3), 1.3 (d, J = 6.9 Hz, 12H, CH(C**H**$_3)_2$), 1.2 (d, J = 6.9 Hz, 12H, CH(C**H**$_3)_2$). ^{13}C{^{1}H} NMR (151 MHz, MeOD) δ 172.7 (N-**C**=O), 154.0 ($C_{pyridyl}$), 152.7 (NH-**(C**=O**)**-NH), 150.4 ($C_{pyridyl}$), 134.8 (C_{phenyl}), 120.0 (C_{phenyl}), 119.9 (C_{phenyl}), 114.7 (C_{phenyl}), 104.5 ($C_{pyridyl}$), 99.0 ($C_{p\text{-}cym}$), 86.8 ($CH_{p\text{-}cym}$), 85.2 ($CH_{p\text{-}cym}$), 84 ($CH_{p\text{-}cym}$), 80.6 ($CH_{p\text{-}cym}$), 61.8 (CH_2- CH_2), 55.8 (CH_2-CH_2), 32.4 (**C**H$(CH_3)_2$), 23.1 (CH(**C**H$_3)_2$), 22.2 (CH(**C**H$_3)_2$), 17.9 (CH_3). ESI-MS: m/z = 497.1 [MRPPU - 4$CF_3SO_3^-$]$^{4+}$, 712.1 [MRPPU - 3$CF_3SO_3^-$]$^{3+}$, 1142.8 [MRPPU - 2$CF_3SO_3^-$]$^{2+}$.

Synthesis and characterization of metalla-assembly MRNPU:

A mixture of [Ru_2(*p*-cymene)$_2${*N,N′*-bis(2-hydroxyethyl)oxamidate}Cl_2] (55 mg, 76.9 μmol) and $AgCF_3SO_3$ (39.5 mg, 153.8 μmol) in anhydrous MeOH (8 mL) was stirred at rt for 2 h. The resulting suspension was then filtered to remove the precipitated AgCl. Subsequently, a solution of 1,1′-(naphthalene-1,5-diyl)bis(3-(pyridin-4-yl) urea) (NPU) (30.6 mg, 76.9 μmol) in a 60 mL solvent mixture of MeOH/ Me_2CO/H_2O (5:2:1, v/v/v) was added to the filtrate. The reaction mixture was heated to 80°C and stirred for 48 h. After completion, the solvent was removed under reduced pressure, and the crude product was dissolved in $CHCl_3$ (2 mL). Slow addition of Et_2O induced precipitation of the target complex as a bright green solid, 86% yield (89 mg, 33.2 μmol). Chemical formula: $C_{100}H_{112}F_{12}N_{16}O_{24}Ru_4S_4$. MW = 2684.3 g·mol^{-1}.

^{1}H NMR (600 MHz, MeOD) δ 8.2 (dd, $J = 19.9, 7.4$ Hz, 4H, $CH_{pyridyl}$), 7.9 (dd, $J = 15.8, 6.5$ Hz, 8H, $CH_{(naphtyl\ +pyridyl)}$), 7.5 (s, 8H, $CH_{naphtyl}$), 7.2–7.0 (m, 8H, $CH_{pyridyl}$), 6.0 (m, 4H, $CH_{p\text{-}cym}$), 5.9 (m, 4H, $CH_{p\text{-}cym}$), 5.5–5.4 (m, 8H, $CH_{p\text{-}cym}$), 4.1 (m, 8H, CH_2), 4.0 (m, 4H, CH_2), 3.9–3.8 (m, 4H, CH_2), 2.8 (m, 4H, $CH(CH_3)_2$), 1.7 (d, $J = 2.5$ Hz, 12H, CH_3), 1.3 (dd, $J = 6.9, 1.0$ Hz, 12H, $CH(CH_3)_2$), 1.2 (dd, $J = 6.9, 1.6$ Hz, 12H, $CH(CH_3)_2$). $^{13}C\{^{1}H\}$ NMR (151 MHz, MeOD) δ 171.4 (N-C=O), 152.8 ($C_{pyridyl}$), 151.9 (NH-(C=O)-NH), 148.9 ($C_{naphtyl}$), 133.1 ($C_{naphtyl}$), 125.1 ($C_{naphtyl}$), 113.3 ($C_{pyridyl}$), 103.2 ($C_{naphtyl}$), 97.5 ($C_{p\text{-}cym}$), 85.7($CH_{p\text{-}cym}$), 83.8 ($CH_{p\text{-}cym}$), 82.7 ($CH_{p\text{-}cym}$), 79.4 ($CH_{p\text{-}cym}$), 60.5 (CH_2- CH_2), 54.5 (CH_2-CH_2), 31.0 ($CH(CH_3)_2$), 21.7 ($CH(CH_3)_2$), 20.8 ($CH(CH_3)_2$), 16.5 (CH_3). ESI-MS: m/z = 522.2 [MRNPU - $4CF_3SO_3^-$]$^{4+}$, 745.8 [MRPPU - $3CF_3SO_3^-$]$^{3+}$, 1193.1 [MRPPU - $2CF_3SO_3^-$]$^{2+}$.

4.4. Preparation of solutions and screening

A 0.1 mM stock solution of metalla-assemblies and fluorescein were prepared in HEPES buffer pH 8, while 0.1 M stock solutions of analytes were prepared in distilled water. Due to the low solubility of adenine, guanine, cytosine, uracil, thymine, stock solutions were prepared in HEPES buffer pH 8. Working solutions of MRPPU, MRNPU, fluorophores, and analytes were obtained by diluting the stock solutions using 20 mM HEPES buffer pH 8. The pH of the HEPES buffer was regulated using solid NaOH and verified with a FiveEasy METTLER TOLEDO® pH meter to ensure precise pH conditions. Screening was conducted using NUNC® 96-well plates, each well was adjusted to a total volume of 100 μL. Pipetting was performed using micropipette for precise and consistent sample distribution in each well. All samples were incubated at 25°C for 10 minutes enabling binding equilibrium for host–guest interactions before measurements. For fluorescein quenching experiments, solutions of metalla-assemblies (100 μM) and fluorescein (100 μM) were used in a 1:1 ratio, affording MR–fluorescein samples with a final MR concentration of 12.5. These samples were subsequently titrated with varying equivalents of analyte solutions (0.01 M) in HEPES buffer pH 8.

4.5. Fluorescence measurements

Fluorescence measurements were conducted using a thermostatted VICTOR® Nivo™ multimode plate reader at 25°C. Fluorescence intensities of fluorescein were measured in black NUNC® 96-well plates using an excitation wavelength of 498 nm and an emission wavelength of 515 nm. Baseline correction of fluorescence values was performed using a blank solution containing only the buffer. All measurements were executed at least in triplicate and analyzed using the GraphPad Prism software version 10.2.3 [76].

4.6. Job Plot analysis for binding stoichiometry

Job plot analysis [78] was performed at 12.5 μM total concentrations of FLU•MR complex, to determine the binding stoichiometry between fluorescein and MR by monitoring changes in the fluorescence intensity as a function of the mole fraction of fluorescein. Stock solutions of fluorescein and MR (100 μM each) were prepared in HEPES buffer pH 8. A series of samples with varying mole fractions of FLU and MR were then prepared, keeping the total concentration (FLU^{2-}•MR complex) constant at 12.5 μM.

4.7. Binding studies

Binding affinity between FLU and MR was determined by fluorescence titrations. A fixed concentration of FLU (12.5 μM) was titrated with increasing concentrations of MR (0–6 equivalents) in HEPES buffer pH 8 and the emission intensities at 515 nm were recorded. The association constants were calculated by fitting the fluorescence data to a 1:1 binding model [79]. The fitting was performed using the following equation [79].

Association constant of FLU^{2-} to the MRPPU and MRNPU:

$$MRPPU + FLU^{2-} \rightleftharpoons FLU^{2-} \subset MRPPU \quad K_{a(MRPPU)} = [FLU^{2-} \subset MRPPU]/[MRPPU][FLU^{2-}]$$

$$MRNPU + FLU^{2-} \rightleftharpoons FLU^{2-}\cdot MRNPU \quad K_{a(MRNPU)} = [FLU^{2-}\cdot MRNPU]/[MRNPU][FLU^{2-}]$$

$$F = F_{free} + \left(F_{bound} - F_{free}\right)\left(\frac{\left(\left[FLU^{2-}\right]_0 + [MR] + \frac{1}{K_a}\right) - \sqrt{\left(\left[FLU^{2-}\right]_0 + [MR] + \frac{1}{K_a}\right)^2 - 4\left[FLU^{2-}\right]_0 + [MR]}}{2\left[FLU^{2-}\right]_0}\right)$$

Where, F is the measured fluorescence signal at a given concentration of MR, F_{free} is the fluorescence of the free FLU (in the absence of MR), F_{bound} is the fluorescence of FLU when it is fully bound to MR (saturation), $[FLU_0^{2-}]$ is the total initial concentration of the fluorescent ligand FLU, [MR] is the concentration of MR added. K_a is the association constant of the FLU^{2-}•MR complex.

Association constant (K_a) is linked to dissociation constant (K_d) by the following equation: $K_a = 1/K_d$.

The binding affinity between FLU^{2-}•MR complex and analytes were performed at 12.5 μM of sensing system FLU^{2-}•MR with increasing concentrations of analytes (0–40 equiv.) in HEPES buffer pH 8. The binding interaction between FLU•MR complex and analytes resulted in two mechanisms: displacement assay or allosteric recognition.

Displacement assay: competitor A:

$$MPPPU + A \rightleftharpoons A \subset MRPPU \quad K_b = [A \subset MRPPU]/[MRPPU].[A] = 1/K_d \text{ (analyte)}$$

$$MRNPU + A \rightleftharpoons A\cdot MRNPU \quad K_b = [A\cdot MRNPU]/[MRNPU].[A] = 1/K_d \text{ (analyte)}$$

$$F = F_{free} + \left(F_{bound} - F_{free}\right)\left(\frac{\left(\left[FLU^{2-}\right]_0 + [MR] + K_d^{app}\right) - \sqrt{\left(\left[FLU^{2-}\right]_0 + [MR] + K_d^{app}\right)^2 - 4\left[FLU^{2-}\right]_0 + [MR]}}{2[MR]}\right)$$

$$K_d^{aap} = K_a\left(1 + \frac{[A]}{K_d(\text{analyte})}\right)$$

Quadratic equation for 1:1 binding model, displacement assay mechanism [79,80]:

Where, $K_d^{app:}$ apparent dissociation constant in the presence of competitor A, K_a is the association constant of FLU to MRPPU or MRNPU, [A]: analyte concentration, $K_{d(analyte)}$: dissociation constant of analyte.

For indicator displacement assay:

$$FLU^{2-} \subset MRPPU + A \rightleftharpoons A \subset MRPPU + FLU^{2-}\ K = [A \subset MRPPU][FLU^{2-}]/[FLU^{2-} \subset MRPPU][A] = K_{a(MRPPU)}/K_b$$

$$FLU^{2-}{\cdot}MRNPU + A \rightleftharpoons A{\cdot}MRNPU + FLU^{2-}\ K = [A{\bullet}MRNPU][FLU^{2-}]/[FLU^{2-}{\bullet}MRNPU][A] = K_{a(MRNPU)}/K_b$$

if: $K<1$, the analyte binds more strongly than FLU^{2-}.

$K>1$, the analyte binds less strongly than FLU^{2-}.

Allosteric recognition:

$$FLU^{2-} \subset MRPPU + A \rightleftharpoons A \subset MRPPU{\cdot}FLU^{2-}$$

$$FLU^{2-}{\cdot}MRNPU + A \rightleftharpoons A{\cdot}MRNPU{\cdot}FLU^{2-}$$

An equation for cooperative binding with an allosteric mechanism [81]:

$$F = F_0 + (F_{max} - F_0) * \left(\frac{[A]^n}{K_d^n + [A]^n}\right)$$

where, F: fluorescence measured at a given concentration of the analyte, F_0: initial fluorescence, F_{max}: fluorescence at saturation, K_d: dissociation constant in μM, [A]: concentration of the analyte, n: degree of cooperativity (Hill coefficient).

Determination of the limit of detection (LOD)

The minimum detectable concentration was determined based on the standard deviation of the blank signal (fluorescence quenching of fluorescein by MR) and the slope of the calibration curve of $FLU^{2-}{\bullet}MR$ with analytes. Fluorescence measurements were recorded for a series of solutions with increasing concentrations of analytes in HEPES buffer pH 8. The LOD was calculated using the equation: $LOD = 3\sigma/S$, where σ is the standard deviation of the blank measurements, and S is the slope of the calibration curve [82].

CRediT authorship contribution statement

Alaa Maatouk: Writing – original draft, Visualization, Data curation. **Thibaud Rossel:** Validation, Supervision. **Bruno Therrien:** Writing – review & editing, Validation, Supervision, Conceptualization.

Declaration of competing interest

The authors declare that they have no known competing financial interests or personal relationships that could have appeared to influence the work reported in this paper.

Supplementary materials

Supplementary material associated with this article can be found, in the online version, at doi:10.1016/j.jorganchem.2026.124029.

Data availability

Data will be made available on request.

References

[1] A. Patel, L. Malinovska, S. Saha, J. Wang, S. Alberti, Y. Krishnan, A.A. Hyman, Science 356 (2017) 753–756, https://doi.org/10.1126/science.aaf6846.
[2] A.V. Gourine, E. Llaudet, N. Dale, K.M. Spyer, Nature 436 (2005) 108–111, https://doi.org/10.1038/nature03690.
[3] J.A. Nirody, I. Budin, P. Rangamani, J. Gen. Physiol. 152 (2020) e201912475, https://doi.org/10.1085/jgp.201912475.
[4] M.H. Pontes, A. Sevostyanova, E.A. Groisman, J. Mol. Biol. 427 (2015) 2586–2594, https://doi.org/10.1016/j.jmb.2015.06.021.
[5] J.H. Kaplan, Annu. Rev. Biochem. 71 (2002) 511–535, https://doi.org/10.1146/annurev.biochem.71.102201.141218.
[6] Q. Wang, Z. Qi, M. Chen, D.H. Qu, Aggregate 2 (2021) e110, https://doi.org/10.1002/agt2.
[7] X. Shen, G. Mizuguchi, A. Hamiche, C. Wu, Nature 406 (2000) 541–544, https://doi.org/10.1038/35020123.
[8] D.G.L. Van Wylen, T.S. Park, R. Rubio, R.M. Berne, J. Cereb, Blood Flow Metab. 6 (1986) 522–528, https://doi.org/10.1038/jcbfm.1986.97.
[9] M.I. Sweeney, Neurosci. Biobehav. Rev. 21 (1997) 207–217, https://doi.org/10.1016/S0149-7634(96)00011-5.
[10] F.A. Bustamante-Barrientos, N. Luque-Campos, M.J. Araya, E. Lara-Barba, J. de Solminihac, C. Pradenas, L. Molina, Y. Herrera-Luna, Y. Utreras-Mendoza, R. Elizondo-Vega, A.M. Vega-Letter, P. Luz-Crawford, J. Transl. Med. 21 (2023) 613, https://doi.org/10.1186/s12967-023-04493-w.
[11] P. Wen, Z. Sun, F. Gou, J. Wang, Q. Fan, D. Zhao, L. Yang, Ageing Res. Rev. 104 (2025) 102667, https://doi.org/10.1016/j.arr.2025.102667.
[12] P. Yu, X. He, L. Zhang, L. Mao, Anal. Chem. 87 (2015) 1373–1380, https://doi.org/10.1021/ac504249k.
[13] Y.F. Huang, H.T. Chang, Anal. Chem. 79 (2007) 4852–4859, https://doi.org/10.1021/ac070023x.
[14] P.J. Xie, M.L. Ye, Z.Y. Hu, G.W. Pan, Y. Zhu, J.J. Zhang, Chin. Chem. Lett. 22 (2011) 1485–1488, https://doi.org/10.1016/j.cclet.2011.09.008.
[15] A. Hellmann, A. Schundner, M. Frick, C. Kranz, Curr. Opin. Electrochem. 39 (2023) 101282, https://doi.org/10.1016/j.coelec.2023.101282.
[16] E.J.C.M. Coolen, I.C.W. Arts, E.L.R. Swennen, A. Bast, M.A. Cohen Stuart, P. C. Dagnelie, J. Chromatogr. B 864 (2008) 43–51, https://doi.org/10.1016/j.jchromb.2008.01.033.
[17] X. Li, X. Gao, W. Shi, H. Ma, Chem. Rev. 114 (2014) 590–659, https://doi.org/10.1021/cr300508p.
[18] Y. Wu, J. Wen, H. Li, S. Sun, Y. Xu, Chin. Chem. Lett. 28 (2017) 1916–1924, https://doi.org/10.1016/j.cclet.2017.09.032.
[19] A.J. Moro, P.J. Cywinski, S. Körsten, G.J. Mohr, Chem. Commun. 46 (2010) 1085–1087, https://doi.org/10.1039/B919661G.
[20] A. Ojida, S.-k Park, Y. Mito-oka, I. Hamachi, Tetrahedron Lett 43 (2002) 6193–6195, https://doi.org/10.1016/S0040-4039(02)01317-5.
[21] D. Bansal, R. Gupta, Dalton Trans. 48 (2019) 14737–14747, https://doi.org/10.1039/C9DT02404B.
[22] J. Wang, X. Gao, J. Ren, B. Song, W. Zhang, J. Yuan, Talanta 286 (2025) 127538, https://doi.org/10.1016/j.talanta.2025.127538.
[23] Y. Kanekiyo, R. Naganawa, H. Tao, Chem. Commun. 2004 (2004) 1006–1007, https://doi.org/10.1039/B400644E.
[24] Y. Suzuki, M. Masuko, T. Hashimoto, T. Hayashita, New J. Chem. 47 (2023) 7035–7040, https://doi.org/10.1039/D3NJ00139C.
[25] I. Carreira-Barral, I. Fernández-Pérez, M. Mato-Iglesias, A. De Blas, C. Platas-Iglesias, D. Esteban-Gómez, Molecules 23 (2018) 479, https://doi.org/10.3390/molecules23020479.
[26] P. Thirupathi, J.Y. Park, L.N. Neupane, M.Y.L.N. Kishore, K.H. Lee, ACS Appl. Mater. Interfaces 7 (2015) 14243–14253, https://doi.org/10.1021/acsami.5b01932.
[27] Z. Xu, N.J. Singh, J. Lim, J. Pan, H.N. Kim, S. Park, K.S. Kim, J. Yoon, J. Am. Chem. Soc. 131 (2009) 15528–15533, https://doi.org/10.1021/ja906855a.
[28] D.T. McQuade, A.E. Pullen, T.M. Swager, Chem. Rev. 100 (2000) 2537–2574, https://doi.org/10.1021/cr9801014.
[29] J.H. Kim, J.H. Ahn, P.W. Barone, H. Jin, J. Zhang, D.A. Heller, M.S. Strano, Angew. Chem. Int. Ed. 49 (2010) 1456–1459, https://doi.org/10.1002/anie.200906251.
[30] L. Wang, L. Yuan, X. Zeng, J. Peng, Y. Ni, J.C. Er, W. Xu, B.K. Agrawalla, D. Su, B. Kim, Y.T. Chang, Angew. Chem. Int. Ed. 55 (2016) 1773–1776, https://doi.org/10.1002/anie.201510003.
[31] P. Srivastava, S.S. Razi, R. Ali, S. Srivastav, S. Patnaik, S. Srikrishna, A. Misra, Biosens. Bioelectron. 69 (2015) 179–185, https://doi.org/10.1016/j.bios.2015.02.028.
[32] J.H. Zhu, C. Yu, Y. Chen, J. Shin, Q.Y. Cao, J.S. Kim, Chem. Commun. 53 (2017) 4342–4345, https://doi.org/10.1039/C7CC01346A.
[33] S. Maji, J. Samanta, R. Natarajan, Chem. Eur. J. 30 (2024) e202303596, https://doi.org/10.1002/chem.202303596.
[34] X. Zhang, Z. Lu, T. Ren, J. Tang, S. Li, C. Zhu, L. Mao, D. Ma, Chin. Chem. Lett. 36 (2025) 110946, https://doi.org/10.1016/j.cclet.2025.110946.
[35] H. Abe, Y. Mawatari, H. Teraoka, K. Fujimoto, M. Inouye, J. Org. Chem. 69 (2004) 495–504, https://doi.org/10.1021/jo035188u.
[36] X. Wu, D. Zhang, S. Deng, J. Wang, C. Yang, D.H. Wang, Y. Bi, Inorg. Chem. Commun. 84 (2017) 195–199, https://doi.org/10.1016/j.inoche.2017.08.025.
[37] P. Shi, Y. Zhang, Z. Yu, S. Zang, Sci. Rep. 7 (2017) 6500, https://doi.org/10.1038/s41598-017-06858-w.
[38] C. Mu, Y. Hou, Z. Zhang, H. Liu, C. Guo, M. Zhang, Fundam. Res. 5 (2025) 2018–2024, https://doi.org/10.1016/j.fmre.2023.03.012.

[39] H. Wu, C. He, Z. Lin, Y. Liu, C. Duan, Inorg. Chem. 48 (2009) 408–410, https://doi.org/10.1021/ic801350h.
[40] F. Zhang, P.J.J. Huang, J. Liu, ACS Sens. 5 (2020) 2885–2893, https://doi.org/10.1021/acssensors.0c01169.
[41] B.T. Huy, D.T. Thangadurai, M. Sharipov, N.N. Nghia, N.V. Cuong, Y.-I. Lee, Microchem. J. 179 (2022) 107511, https://doi.org/10.1016/j.microc.2022.107511.
[42] S. Sivagnanam, P. Mahato, P. Das, Org. Biomol. Chem. 21 (2023) 3942–3983, https://doi.org/10.1039/D3OB00209H.
[43] J. Krämer, R. Kang, L.M. Grimm, L. De Cola, P. Picchetti, F. Biedermann, Chem. Rev. 122 (2022) 3459–3636, https://doi.org/10.1021/acs.chemrev.1c00746.
[44] A.C. Sedgwick, J.T. Brewster II, T. Wu, X. Feng, S.D. Bull, X. Qian, J.L. Sessler, T. D. James, E.V. Anslyn, X. Sun, Chem. Soc. Rev. 50 (2021) 9–38, https://doi.org/10.1039/C9CS00538B.
[45] K.S. Suslick, N.A. Rakow, A. Sen, Tetrahedron 60 (2004) 11133–11138, https://doi.org/10.1016/j.tet.2004.09.007.
[46] J.J. Lavigne, E.V. Anslyn, Angew. Chem. Int. Ed. 40 (2001) 3118–3130, https://doi.org/10.1002/1521-3773(20010903)40:17<3118::AID-ANIE3118>3.0.CO;2-Y.
[47] T.M. Swager, Acc. Chem. Res. 31 (1998) 201–207, https://doi.org/10.1021/ar9600502.
[48] J.I. Abdul Rashid, N.A. Yusof, Sens. Bio-Sens. Res. 16 (2017) 19–31, https://doi.org/10.1016/j.sbsr.2017.09.001.
[49] L. You, D. Zha, E.V. Anslyn, Chem. Rev. 115 (2015) 7840–7892, https://doi.org/10.1021/cr5005524.
[50] D.F.N. Agatra, D. Marutho, J. Intell. Comput. Health Inform. 6 (2025) 18–27, https://doi.org/10.26714/jichi.v6i1.16176.
[51] A.T. Wright, E.V. Anslyn, Chem. Soc. Rev. 35 (2006) 14–28, https://doi.org/10.1039/B505518K.
[52] A.M. Martinez, A.C. Kak, IEEE Trans. Pattern Anal. Mach. Intell. 23 (2001) 228–233, https://doi.org/10.1109/34.908974.
[53] L. Feng, C.J. Musto, J.W. Kemling, S.H. Lim, K.S. Suslick, Chem. Commun. 46 (2010) 2037–2039, https://doi.org/10.1039/B926848K.
[54] S.E. Schneider, S.N. O'Neil, E.V. Anslyn, J. Am. Chem. Soc. 122 (2000) 542–543, https://doi.org/10.1021/ja9935153.
[55] W. Li, X. Gong, X. Fan, S. Yin, D. Su, X. Zhang, L. Yuan, Chin. Chem. Lett. 30 (2019) 1775–1790, https://doi.org/10.1016/j.cclet.2019.07.056.
[56] A.M. Agafontsev, A. Ravi, T.A. Shumilova, A.S. Oshchepkov, E.A. Kataev, Chem. Eur. J. 25 (2019) 2684–2694, https://doi.org/10.1002/chem.201802978.
[57] S.J. Butler, K.A. Jolliffe, ChemPlusChem 86 (2021) 59–70, https://doi.org/10.1002/cplu.202000567.
[58] S.C. McCleskey, M.J. Griffin, S.E. Schneider, J.T. McDevitt, E.V. Anslyn, J. Am. Chem. Soc. 125 (2003) 1114–1115, https://doi.org/10.1021/ja021230b.
[59] P.P. Neelakandan, M. Hariharan, D. Ramaiah, J. Am. Chem. Soc. 128 (2006) 11334–11335, https://doi.org/10.1021/ja062651m.
[60] X. Chen, M.J. Jou, J. Yoon, Org. Lett. 11 (2009) 2181–2184, https://doi.org/10.1021/ol9004849.
[61] J.M. Roberts, B.M. Fini, A.A. Sarjeant, O.K. Farha, J.T. Hupp, K.A. Scheidt, J. Am. Chem. Soc. 134 (2012) 3334–3337, https://doi.org/10.1021/ja2108118.
[62] P. Howlader, P. Das, E. Zangrando, P.S. Mukherjee, J. Am. Chem. Soc. 138 (2016) 1668–1676, https://doi.org/10.1021/jacs.5b12237.
[63] R.N. Dsouza, U. Pischel, W.M. Nau, Chem. Rev. 111 (2011) 7941–7980, https://doi.org/10.1021/cr200213s.
[64] T.J.P. Hersbach, C. Rabin, J. Phys. Chem. B 126 (2022) 9632–9642, https://doi.org/10.1021/acs.jpcb.2c06288.
[65] T. Xiong, Y. Zhang, L. Donà, M. Gutiérrez, A.F. Möslein, A.S. Babal, N. Amin, B. Civalleri, J.-C. Tan, A.C.S. Appl, Nano Mater. 4 (2021) 10321–10333, https://doi.org/10.48550/arXiv.2109.12032.
[66] M.D. Ludden, M.D. Ward, Dalton Trans. 50 (2021) 2782–2791, https://doi.org/10.1039/D0DT04211K.
[67] M. Rajasekar, J. Mol. Struct. 1224 (2021) 129085, https://doi.org/10.1016/j.molstruc.2020.129085.
[68] B.T. Nguyen, E.V. Anslyn, Coord. Chem. Rev. 250 (2006) 3118–3127, https://doi.org/10.1016/j.ccr.2006.04.009.
[69] Z. Xu, D.R. Spring, J. Yoon, Chem. Asian J. 6 (2011) 2114–2122, https://doi.org/10.1002/asia.201100120.
[70] Y. Suzuki, M. Masuko, T. Hashimoto, T. Hayashita, New J. Chem. 47 (2023) 7035–7040, https://doi.org/10.1039/D3NJ00139C.
[71] P. Arranz-Mascarós, C. Bazzicalupi, A. Bianchi, C. Giorgi, M.L. Godino-Salido, M. D. Gutiérrez-Valero, R. Lopez-Garzón, B. Valtancoli, New J. Chem. 35 (2011) 1883–1891, https://doi.org/10.1039/C1NJ20393B.
[72] R. Biswas, S. Ghosh, S.K. Bhaumik, S. Banerjee, Beilstein J. Org. Chem. 16 (2020) 2728–2738, https://doi.org/10.3762/bjoc.16.223.
[73] A.M. Agafontsev, T.A. Shumilova, A.S. Oshchepkov, F. Hampel, E.A. Kataev, Chem. Eur. J. 26 (2020) 9991–9997, https://doi.org/10.1002/chem.202001523.
[74] B.S. Morozov, A.S. Oshchepkov, I. Klemt, A.M. Agafontsev, S. Krishna, F. Hampel, H.-G. Xu, A. Mokhir, D. Guldi, E. Kataev, JACS Au 3 (2023) 964–977, https://doi.org/10.1021/jacsau.2c00658.
[75] A. Maatouk, T. Rossel, B. Therrien, Inorganics 13 (2025) 1, https://doi.org/10.3390/inorganics13010001.
[76] GraphPad Software, Inc. GraphPad Prism Version 10.2.3 for Windows. Boston (MA): GraphPad Software; Available from: https://www.graphpad.com.
[77] A. Garci, A.A. Dobrov, T. Riedel, E. Orhan, P.J. Dyson, V.B. Arion, B. Therrien, Organometallics 33 (2014) 3813–3822, https://doi.org/10.1021/om5005176.
[78] F. Ulatowski, K. Dąbrowa, T. Bałakier, J. Jurczak, J. Org. Chem. 81 (2016) 1746–1756, https://doi.org/10.1021/acs.joc.5b02909.
[79] P. Thordarson, Chem. Soc. Rev. 40 (2011) 1305–1323, https://doi.org/10.1039/C0CS00062K.
[80] W. Yu, J. Qiang, J. Yin, S. Kambam, F. Wang, Y. Wang, X. Chen, Org. Lett. 16 (2014) 2220–2223, https://doi.org/10.1021/ol5007339.
[81] A. Dyachenko, R. Gruber, L. Shimon, M. Sharon, Proc. Natl. Acad. Sci. U. S. A. 110 (2013) 7235–7239, https://doi.org/10.1073/pnas.1302395110.
[82] Analytical Methods Committee, Analyst 112 (1987) 199–204, https://doi.org/10.1039/AN9871200199.